Laminar dependence of neuronal correlations in visual cortex

Matthew A. Smith,[1] Xiaoxuan Jia,[2]* Amin Zandvakili,[2]* and Adam Kohn[2,3]

[1]*Departments of Ophthalmology and Bioengineering, Center for the Neural Basis of Cognition and Fox Center for Vision Restoration, University of Pittsburgh, Pittsburgh, Pennsylvania;* [2]*Dominick Purpura Department of Neuroscience, Albert Einstein College of Medicine, Bronx, New York; and* [3]*Department of Ophthalmology and Visual Sciences, Albert Einstein College of Medicine, Bronx, New York*

Smith MA, Jia X, Zandvakili A, Kohn A. Laminar dependence of neuronal correlations in visual cortex. *J Neurophysiol* 109: 940–947, 2013. First published November 28, 2012; doi:10.1152/jn.00846.2012.—Neuronal responses are correlated on a range of timescales. Correlations can affect population coding and may play an important role in cortical function. Correlations are known to depend on stimulus drive, behavioral context, and experience, but the mechanisms that determine their properties are poorly understood. Here we make use of the laminar organization of cortex, with its variations in sources of input, local circuit architecture, and neuronal properties, to test whether networks engaged in similar functions but with distinct properties generate different patterns of correlation. We find that slow timescale correlations are prominent in the superficial and deep layers of primary visual cortex (V1) of macaque monkeys, but near zero in the middle layers. Brief timescale correlation (synchrony), on the other hand, was slightly stronger in the middle layers of V1, although evident at most cortical depths. Laminar variations were also apparent in the power of the local field potential, with a complementary pattern for low frequency (<10 Hz) and gamma (30–50 Hz) power. Recordings in area V2 revealed a laminar dependence similar to V1 for synchrony, but slow timescale correlations were not different between the input layers and nearby locations. Our results reveal that cortical circuits in different laminae can generate remarkably different patterns of correlations, despite being tightly interconnected.

cortical layers; neuronal correlation; population coding; V1; visual cortex

SPIKE TIMING AND FIRING RATES are correlated between nearby neurons that have similar functional properties (Cohen and Kohn, 2011). Rate correlations can strongly affect population coding (Zohary et al., 1994; Averbeck et al., 2006; Graf et al., 2011), and spike timing correlation has been proposed to play a role in cortical function (Gray, 1999; Fries, 2009). Correlations can arise from common input to a pair of cells from a presynaptic neuron or pool of neurons. However, modeling work has shown that correlations can be near zero, even in highly recurrent networks, if excitatory and inhibitory inputs are balanced appropriately (Salinas and Sejnowski, 2000; Renart et al., 2010). The mechanisms generating correlations are thus not straightforward, and how correlations depend on network architecture and the intrinsic properties of neurons remains unclear. This has limited our understanding of why correlations vary across brain areas and how stimulus conditions and behavioral states modulate correlations (Cohen and Kohn, 2011).

The laminar organization of cortex provides an opportunity to compare correlations in networks engaged in similar computations but with distinct properties. First, circuit architecture differs among layers. For instance, the middle layers (layers 4C alpha and beta) of primary visual cortex (V1) are driven by feed-forward input from the thalamus and have recurrent circuitry of a limited spatial extent (Lund et al., 1979; Blasdel and Lund, 1983). In the superficial and deep layers, neurons are richly interconnected, in part by horizontal connections known to extend for several millimeters (Gilbert and Wiesel, 1983). Second, the electrophysiological properties of neurons and synapses vary across layers, due to the expression of different receptors and ion channels (Markram et al., 2004; Nelson et al., 2006; Thomson and Lamy, 2007). Finally, layers generate different rhythmic fluctuations, which are observable in the local field potential (LFP) (Roopun et al., 2006; Bollimunta et al., 2008; Maier et al., 2010; Minlebaev et al., 2011; Xing et al., 2012) and may contribute to correlations (Kohn et al., 2009). Here we test whether these different properties of laminar circuits give rise to distinct patterns of correlation.

This manuscript was published previously in abstract form (Smith and Kohn, 2009).

MATERIALS AND METHODS

We recorded data from nine anesthetized, adult male macaque monkeys (*Macaca fascicularis*), by previously described methods (Smith and Kohn, 2008). In brief, anesthesia was induced with ketamine (10 mg/kg) and maintained during preparatory surgery with isoflurane (1.0–2.0% in 95% O_2). Anesthesia during recordings was maintained with sufentanil citrate (6–18 μg·kg^{-1}·h^{-1}). Vecuronium or pancuronium bromide (0.1–0.15 mg·kg^{-1}·h^{-1}) was used to suppress eye movements. Physiological signs were monitored to ensure adequate anesthesia and animal well-being. We used supplementary lenses to bring the retinal image into focus. At the end of the recording session, animals were killed and tissue was processed histologically to verify recording locations. All procedures were approved by the Institutional Animal Care and Use Committee of the Albert Einstein College of Medicine.

We recorded in V1 with a group of five to seven linearly arranged (305 μm spacing) platinum-tungsten electrodes or tetrodes (Thomas Recording), inserted normally to the cortical surface. The electrodes were aligned by use of a microscope to the end of the guide tube and advanced together through cortex, sampling in 200 μm intervals until all electrodes had exited into white matter. Neuronal receptive fields were within 5° of the fovea.

V2 recordings were performed by angling the electrodes 20° from vertical, in the sagittal plane, and advancing through V1 into the white matter. We performed V2 recordings while monitoring the activity of a population of neurons in the superficial layers of V1, using "Utah" microelectrode array recordings (described in Smith and Kohn, 2008).

* X. Jia and Amin Zandvakili contributed equally to this work.

Address for reprint requests and other correspondence: M. A. Smith, Dept. of Ophthalmology, Univ. of Pittsburgh, 203 Lothrop St., Eye and Ear Inst., Rm. 914, Pittsburgh, PA 15213 (e-mail: smithma@pitt.edu).

Signals were band-pass filtered between 0.3 and 10 kHz and sampled at 40 kHz. Waveform segments that exceeded a user-defined threshold were sorted offline (Plexon Offline Sorter). We quantified sort quality using the signal-to-noise ratio (SNR) of each candidate unit (Kelly et al., 2007), keeping units with an SNR of at least 2.3 and a response of at least 2 sp/s to the best grating stimulus (502 units in V1 and 122 in V2). Changing the SNR or responsivity threshold did not qualitatively change any of the results described herein. The LFP was obtained by band-pass filtering the raw signal (0.3–250 Hz) and sampling at 1 kHz.

Visual stimulation. Stimuli were generated with EXPO and displayed on a linearized CRT monitor (mean luminance 40 cd/m^2, 110 cm from the animal) with a resolution of 1,024 by 768 pixels and a refresh rate of 100 Hz. Stimuli were presented in a circular aperture surrounded by a gray field of average luminance. We mapped the spatial receptive field (RF) of units by presenting small (0.6°) drifting gratings at a range of spatial positions. We then centered our stimuli on the aggregate RF of the recorded units. Stimuli were viewed binocularly and presented for 1.28 s, separated by 1.5 s intervals of isoluminant gray screen (except in one penetration, for which the interval was 10 s). We presented full-contrast drifting sinusoidal gratings at 8 or 12 orientations spaced equally (22.5 or 30° increments). The spatial frequency (1–1.3 cpd) and temporal frequency (3 or 6.25 Hz) values were chosen to correspond to the typical preference of parafoveal V1 neurons (De Valois et al., 1982) and were held constant across sites in the same penetration. The position and size (3.9–5.3°) of the grating were sufficient to cover the receptive fields of all the neurons. We use the smallest stimulus that covered the receptive fields for both eyes. When the eyes were not aligned, we used two smaller stimuli, each covering the receptive fields for one eye. Stimulus orientation was block randomized, and blocks were repeated 30–100 times.

Analysis. We paired each neuron with all other simultaneously recorded neurons, excluding pairs from the same electrode or tetrode. This resulted in 3,247 pairs of V1 neurons recorded from 43 electrode or tetrode tracks, grouped in eight ensemble penetrations recorded in five hemispheres of four animals. For V2, we made nine penetrations in seven hemispheres of seven animals (five new animals with respect to the V1 data). In some of these penetrations we recorded at one or two sites, targeting the input layers. In total we recorded 230 pairs of V2 neurons at 18 distinct sites.

For each stimulus orientation, we Z-scored the spike counts of each neuron. We calculated spike count correlations (r_{sc}) for each pair after combining responses to all stimuli, except we removed trials on which the response of either neuron was >3 SDs different from its mean (Zohary et al., 1994) to avoid contamination by outlier responses.

We computed the cross-correlogram (CCG) for each stimulus condition and pair, and corrected it using an all-way shuffle correction. CCGs were normalized by the geometric mean spike rate. To isolate the narrow peak of the CCGs we used a jitter correction method (Amarasingham et al., 2012) with a window of 10 ms, removing all correlation on a timescale greater than that window size. We then averaged CCGs across stimulus conditions. We smoothed these CCGs with a Gaussian kernel (SD = 1.0 ms) before further analysis. A more detailed discussion of these measures of correlation can be found in (Kohn and Smith, 2005; Smith and Kohn, 2008).

We performed current source density (CSD) analysis by computing the average evoked (stimulus-locked) LFP at each site, smoothing these signals across sites, and then calculated the second spatial derivative (Stoelzel et al., 2009). We then averaged the CSDs across electrodes of a single penetration and determined the minimum value of the CSD in the first 100 ms. We defined the middle layer sink to be the depth and time that first reached 40% of that value, if this was followed by a source (reaching at least 50% of the maximum CSD value and occurring within 100 ms of the sink). For one of the eight penetrations, this method did not provide a clear assignment of the

middle layers, and for another we collected only spiking activity and no LFP.

For LFP spectral analysis, we used LFPs acquired from all depths at which we recorded single neurons that met the criteria discussed above. We calculated the spectrum for each trial separately and then averaged across trials and stimuli. We then normalized the average spectrum from each electrode to unity area prior to analysis, because of differences in raw LFP amplitude across some electrodes. We did not calculate power with respect to that observed under spontaneous conditions because we wished to measure effects over a broad frequency range, for which some frequencies were suppressed and some enhanced relative to the spontaneous LFP.

For V2 recordings, we first calculated CCGs between every pairing of V1 and V2 neurons and then averaged across all conditions and pairs. We defined the input layers to be those V2 sites at which we observed evidence that neurons received direct input from V1 (Tanaka, 1983; Reid and Alonso, 1995): namely, that the average jitter-corrected CCG had a significant peak within 10 ms of 0 ms time lag (defined as 5 SDs above the value at time lags of ±75–125 ms). V2 recording sites were defined to be deep/superficial, if the average CCGs lacked a sharp peak and these sites were recorded before/after an input layer site. We applied the same rate and sort quality criteria as for our V1 data.

All indications of variation in the graphs and text are SE. The statistical significance of all results was evaluated with two-tailed *t*-tests, unless otherwise noted. Significance of r_{sc} was assessed after applying the Fisher Z-transform to the data.

RESULTS

We recorded from pairs of V1 neurons in anesthetized macaque monkeys, using bundles of electrodes and tetrodes that we lowered through cortex in penetrations orthogonal to the pial surface. We sampled sequentially and systematically across the cortical depth, with an intersite distance of 200 μm.

We used drifting sinusoidal gratings, of sufficient size to cover the receptive fields of all recorded units, to evoke activity. From these responses, we calculated r_{sc} between all pairs of neurons recorded at each depth, using counts measured during the full presentation epoch (1.28 s). Figure 1*A* shows the average r_{sc} values for neuronal pairs grouped by recording depth, for two sample penetrations. We found r_{sc} had consistently higher values at superficial (top) and deep (bottom) sites and was near zero in between.

In total, we performed eight ensemble penetrations (43 electrode or tetrode tracks). We aligned these based on the last site prior to entering white matter (WM) because alignment to the cortical surface was affected by the variable responsiveness of the exposed brain tissue. This alignment revealed a weak mean value of r_{sc} roughly 0.8 mm above the layer 6/WM border, consistent with the example penetrations in Fig. 1*A*. Previous histological studies show this location corresponds to the expected depth and width (300–400 μm) of layer 4C in V1 (Fitzpatrick et al., 1985; Lund, 1988). We therefore termed this location (0.8 mm from the last recording site) the middle layers and sites above and below it as in the superficial and deep layers, respectively. The cumulative distributions (Fig. 1*B*) and frequency histograms (right) of r_{sc} were significantly different across these groups. The mean r_{sc} value was 0.112 ± 0.005, 0.014 ± 0.012 and 0.073 ± 0.007 for the superficial (*n* = 1,613), middle (*n* = 469) and deep layers (*n* = 1,165), respectively (*P* < 0.001 for all comparisons among groups).

To provide independent verification that the sites with low mean values of r_{sc} were in the middle layers, we analyzed LFPs, which we recorded in most penetrations simultaneously
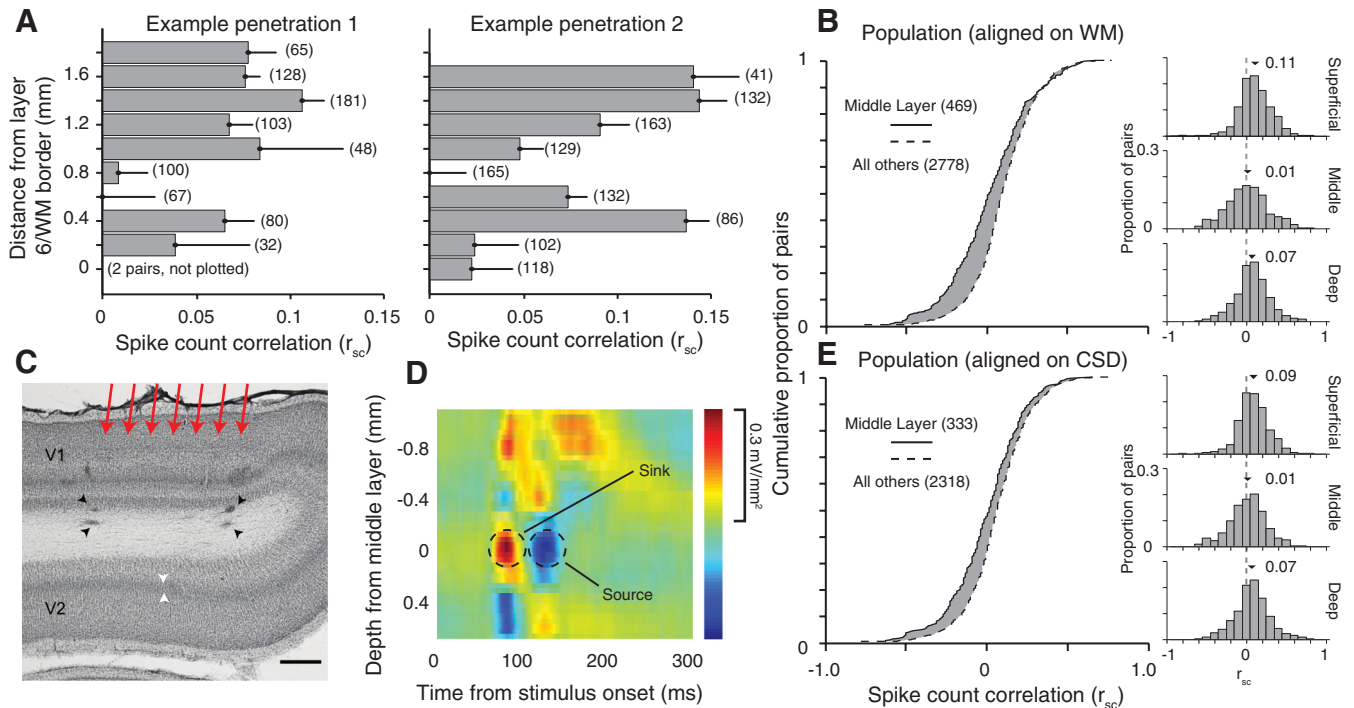
Fig. 1. Dependence of spike count correction (r_{sc}) on laminar location. *A*: mean r_{sc} values for at sequentially recorded sites, in 2 orthogonal penetrations traversing the layers of cortex. Error bars indicate +1 SE. The number of pairs for each bin are indicated in parentheses to the *right* of that bin. No bar is plotted for depth 0 in the *left* example because only 2 pairs were recorded at this depth. *B*: cumulative distributions of r_{sc} for all sites with a recording depth of 0.8 mm above the final site with spiking activity (solid line) and other locations (dashed line). Histograms for r_{sc} values at superficial, middle, deep layer sites shown to the right. *C*: a Nissl-stained section from an example penetration in V1. The 4 black arrowheads indicate lesions made by electrodes at the ends of the linear array, at the last recording site in V1 and again 250 μm into white matter. The red arrows indicate the rough arrangement of the electrodes in this V1 penetration. The white arrowheads indicate the location of layer 4 in V2. The scale bar indicates 500 μm (uncorrected for tissue shrinkage). *D*: a current source density (CSD) analysis of the LFP signals from an individual penetration. Sinks are shown in red and sources in blue. The middle layers are identifiable as the earliest current sink followed by a source (indicated by dashed circles). For display purposes only, this CSD was upsampled 5 times and then smoothed with a 3 × 3 boxcar filter. *E*: as in *B*, but with the middle layers defined by the site of the early sink/source of the CSD analysis.

with spiking activity. From the LFP we calculated the CSD profile for each penetration. CSD analysis reveals the location, direction, and strength of current flow and is widely used to distinguish the laminar location of recording sites (Givre et al., 1995; Schroeder et al., 1998; Rajkai et al., 2008; Maier et al., 2010). The earliest current sink is found in layer 4C (red in Fig. 1*D*), where input from the lateral geniculate nucleus (LGN) arrives, and activation in superficial and deep layers follows. Although CSD analysis is typically performed on data recorded simultaneously across cortical layers, this is not required as the analysis is based on signals that are averaged across trials.

Our CSD analysis provided clear sinks in six of the eight recorded penetrations (see MATERIALS AND METHODS for criteria) and these were confined to one to two recording sites, consistent with the thickness of layer 4C (Fitzpatrick et al., 1985; Lund, 1988). We aligned the data from these six penetrations based on the site of the most prominent sink and defined this site (the single depth with the strongest sink) as in the middle layers. Using this CSD-based designation (Fig. 1*E*), we found that r_{sc} was higher at superficial (0.097 ± 0.003, n = 1,347 pairs, P = 1.2 × 10^{-10}) and deep sites (0.076 ± 0.006, n = 971, P = 1.2 × 10^{-4}) than in the middle layers (0.018 ± 0.018, n = 333). The mean value of r_{sc} in the middle layers was not significantly different from zero (P = 0.27). Thus, CSD analysis confirmed that the site of low correlations, evident when data were aligned by final site at which neuronal activity could be detected, was in the middle layers.

As a third method to confirm the laminar location of our recording sites, we made and recovered electrolytic lesions in three of the eight penetrations. We made lesions only at the final recording sites and again 200–300 μm into the WM, so as not to influence the recorded responses. In each case, the recovered lesions were at the expected locations, as shown for one section in Fig. 1*C* (black arrowheads).

Variations in mean values of r_{sc} could reflect interesting difference across laminar circuits, but they could also arise for more pedestrian reasons. For instance, when the firing rate of either neuron in a pair is low, r_{sc} will be small, even when the underlying membrane potentials are strongly correlated (de la Rocha et al., 2007; Cohen and Kohn, 2011). We therefore compared mean firing rates across all 12 orientations at each location. We found higher mean rates for neurons in the middle than superficial and deep layers (13.5 ± 2.05, n = 60 vs. 10.2 ± 0.50 sp/s, n = 442, P = 0.04), consistent with previous studies (Gur et al., 2005). Furthermore, when we considered only cases in which both neurons had a mean firing rate of at least 5 sp/s, r_{sc} in the middle layers was 0.003 ± 0.018 compared with 0.076 ± 0.006 in the other layers (P = 0.0003). Thus, the weak correlations in the middle layers are not due to low rates there.

A second explanation for weak middle layer correlations is that the sampled neurons have more diverse functional properties than those sampled in other layers: correlations are typically stronger between neurons with similar response properties (Zohary et al., 1994; Bair et al., 2001; Kohn and Smith, 2005; Smith and Kohn,

A Shuffle-corrected

B Jitter-corrected
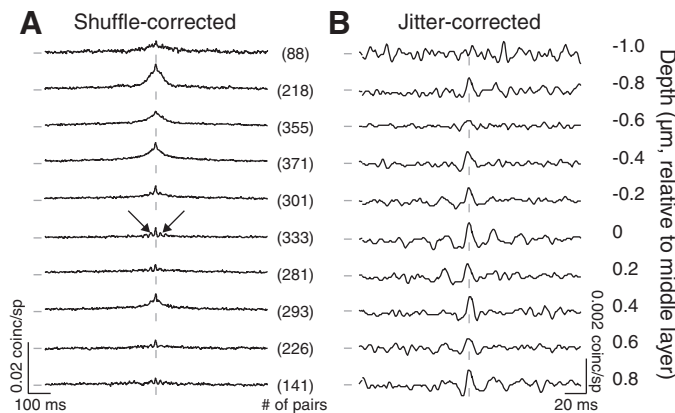
Fig. 2. Dependence of timing correlations on laminar location. *A*: average shuffle-corrected CCGs for pairs of neurons grouped by recording depth (shown at the right). The tick marks to the left of the CCGs indicate a value of 0 coinc./sp; those at the bottom of the CCGs indicate zero time lag. Vertical and horizontal scale bars are shown separately for each panel. The number of pairs recorded at each depth are indicated between the panels. Two depths, -1.2 and 1.0 mm, are not plotted because they had too few pairs (14 and 30, respectively). Arrows indicate oscillatory side lobes. *B*: average jitter-corrected CCGs for the same data as in *A*. The axes scales are adjusted for clearer display.

2008). We quantified the similarity of orientation tuning of each pair by Pearson's correlation (signal correlation). Signal correlations for the middle layers (-0.039 ± 0.022, $n = 333$) were slightly smaller than at other sites (0.053 ± 0.009, $n = 2,318$, $P = 0.0003$). However, even among pairs with high signal correlation (>0.5), indicating similar tuning, r_{sc} was low in the middle layers (0.051 ± 0.033, $n = 38$), and smaller than in other layers (0.110 ± 0.010, $n = 420$), although this difference was not statistically significant ($P = 0.097$). Weak correlations in middle layers are thus not due to lower signal correlations among the sampled neurons. Note that although r_{sc} was weak in the middle layers, values were larger for pairs with similar tuning (0.051 compared with 0.014 on average), similar to the dependence reported in the superficial layers (Smith and Kohn, 2008). We further performed a multivariate regression, incorporating mean firing rate, signal correlation, and layer (as a dummy variable, with the middle layers having a value of 1 and superficial and deep layers having a value of zero) as factors to explain variations in r_{sc} ($R^2 = 0.024$, $P = 4.8 \times 10^{-14}$). Each factor added predictive power to the model (coefficients of 0.033 for rate, 0.002 for signal correlation, and -0.070 for layer, all with 95% confidence intervals that did not overlap zero), suggesting they each influence the strength of r_{sc}. Furthermore, while firing rate and tuning similarity influence correlations, the regression model suggests they are not able to explain the reduction in r_{sc} we observed in the middle layers.

Laminar trends in spike timing correlation and the LFP. We have previously shown that spike count correlations measured in long response epochs arise primarily from slow cofluctuations of rate, with a weaker contribution from near synchronous spikes (Kohn and Smith, 2005; Smith and Kohn, 2008). These contributions are evident as broad and narrow peaks in the spike train CCG, respectively. To explore the laminar dependence of spike timing correlations, we computed the shuffle-corrected CCG for each pair and averaged CCGs from all pairs recorded at each depth, aligned by the CSD (Fig. 2*A*).

CCGs in the superficial and deep layers had broad central peaks, but these were absent in the middle layers. This is consistent with the laminar variations in r_{sc}, since r_{sc} is proportional to the integral of the CCG (Bair et al., 2001). The CCGs in the middle layers were also notable for oscillatory side lobes around the peak (arrows in Fig. 2*A*), in the gamma range (30–50 Hz); the gamma power in the CCG (calculated within 100 ms of zero time lag) was significantly higher for pairs in the middle than superficial ($P = 1.2 \times 10^{-7}$) and deep ($P = 3.2 \times 10^{-4}$) layers.

To isolate synchronous activity from slower cofluctuations, we used a previously described method of correcting the raw CCG of each pair with a predictor derived from jittered data (10 ms jitter window; see MATERIALS AND METHODS). The most prominent peaks in these jitter-corrected CCGs were in the middle layers (Fig. 2*B*, note change in scale). Synchrony, measured as the area under the jitter-corrected CCG within 5 ms of zero time lag, was higher in the middle ($7.9 \pm 1.3 \times 10^{-4}$ coinc./sp) than the superficial ($5.8 \times 10^{-4} \pm 5.2 \times 10^{-5}$, $P = 0.088$) and deep layers ($6.0 \times 10^{-4} \pm 6.9 \times 10^{-5}$, $P = 0.182$), although this difference did not reach statistical significance. The peak height of the CCG at zero time lag, however, was significantly higher in the middle layers ($7.0 \times 10^{-4} \pm 2.5 \times 10^{-5}$ coinc./sp) compared with the superficial ($6.5 \times 10^{-4} \pm 7.9 \times 10^{-6}$, $P = 0.007$) and deep layers ($6.4 \times 10^{-4} \pm 1.1 \times 10^{-5}$, $P = 0.009$).

The frequency content of the LFP is known to vary with cortical depth (Roopun et al., 2006; Minlebaev et al., 2011; Xing et al., 2012). Low frequency cortical rhythms are thought to contribute to slow timescale correlations (Kohn and Smith, 2005; Poulet and Petersen, 2008; Smith and Kohn, 2008; Kohn et al., 2009; Mitchell et al., 2009; Kelly et al., 2010), whereas higher frequency rhythms (e.g., gamma) have been associated with brief timescale spike timing correlations (Samonds and Bonds, 2005; Fries et al., 2008). We therefore determined whether the laminar dependence of r_{sc} and timing correlations were also reflected in the LFP.

We measured normalized LFP power for frequencies from 0–80 Hz and found substantial laminar variation. Low frequency (0–10 Hz) power was a dominant component of the LFP across the cortical layers, with a peak in layer 6 and weaker values in the middle and very superficial layers (Fig. 3*A*). The proportion of power in the gamma frequencies (30–50 Hz) was highest in the middle and superficial layers (Fig. 3*B*), consistent with most
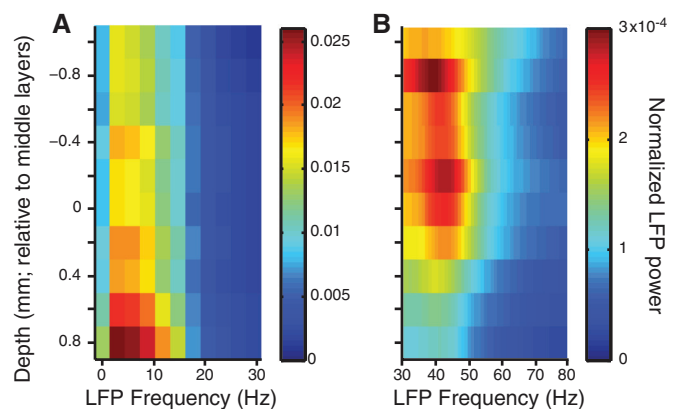
Fig. 3. Dependence of local field potential (LFP) power on laminar location. *A*: normalized LFP power in the 0–30 Hz range, as a function of electrode depth (*y*-axis) and frequency (*x*-axis). *B*: LFP power in the 30–80 Hz band. Note the change in scale compared with *A*.

(Roopun et al., 2006; Minlebaev et al., 2011; Xing et al., 2012) but not all previous reports (Maier et al., 2010). For all pairs, we compared spiking correlations with the average LFP power measured at the two electrodes. The value of r_{sc} was correlated with low-frequency ($r = 0.07$, $P = 6.7 \times 10^{-4}$) but not gamma power ($r = -0.02$, $P = 0.97$). Synchrony, measured as the area under the jitter-corrected CCG, was correlated with gamma ($r = 0.17$, $P = 4.1 \times 10^{-19}$) but not low-frequency power ($r = -0.01$, $P = 0.72$).

Thus, we find that LFP frequency content has a different laminar distribution depending on the frequency band, and there is some tendency for the measures of spiking correlation on fast (synchrony) and slow (r_{sc}) timescales to mirror the trends in the gamma and low frequency bands in LFP power, respectively.

Laminar trends outside V1. We next sought to test whether the weak mean r_{sc} in the middle layers of V1 represents a special property of V1 or a general principle that circuitry in the input layers minimizes slow timescale correlations. For this purpose, we performed additional recordings of 230 pairs of neurons in V2. This included a total of nine electrode penetrations in seven animals, two of which sampled across all layers of V2 and the rest targeted one to three sites in or near the input layers. These data were culled from a larger set of V2 data collected for other experimental purposes.

In extrastriate cortex, CSD analysis reveals more diverse patterns and its relationship to laminar structure is less well established (Schroeder et al., 1998). Furthermore, because we wished to match the eccentricity of our recordings in V1, we recorded in a portion of V2 that was buried in the posterior bank of the lunate sulcus, making it difficult to ensure orthogonal penetrations. Therefore, we used an alternative strategy for determining the location of the inputs layers: we measured whether a particular location in V2 received input from V1 by pairing our V2 recordings (made with five to seven microelec-

trodes or tetrodes, advanced as a group) with microelectrode array recordings in the superficial layers of V1. We then calculate the spike-train CCGs between all V1-V2 pairings, to test for evidence of a functional interaction between them (Tanaka, 1983; Reid and Alonso, 1995).

The average jitter-corrected V1-V2 CCGs for nine recording sites sampled sequentially across V2 layers in a single penetration are shown in Fig. 4A. At deep (bottom) and superficial (top) sites, CCGs did not have sharp peaks. At intermediate locations-typically at two or three sites-sharp peaks were evident (red). These were offset from 0 ms time lag (V1 firing before V2), by 2.2 ms on average. These peaks were observed only when the V1 and V2 spatial receptive fields were precisely aligned (center-to-center spacing of <1°) and at nominal depths typically $400-800$ μm from the layer 6/WM border (Zandvakili and Kohn, 2010), consistent with the expected location of V1 terminals in layer 4 and deep layer 3 of V2 (Van Essen et al., 1986; Rockland and Virga, 1990) (see white arrowheads in Fig. 1C for location of layer 4). We interpret these peaks as indicating a functional connection from V1 to V2 (Reid and Alonso, 1995; Zandvakili and Kohn, 2010) and defined those sites at which we observed a sharp peak in the average V1-V2 CCG (across all pairs and stimulus orientations) as being in the input layers of V2. In two penetrations, electrolytic lesions performed after the recordings confirmed that the first recorded site was near the layer 6/WM border, and that the locations with sharp peaks were centered in the middle layers.

We then measured correlations among V2-V2 pairs recorded simultaneously at each depth. In contrast to our observations in V1, we found no evidence for r_{sc} to differ significantly across layers (Fig. 4B). In layers with sharp peaks, the mean r_{sc} (0.162 ± 0.014) was not different from that in the other layers (0.153 ± 0.010, $P = 0.54$), and it was significantly >0 ($P = 5.5 \times 10^{-21}$). The mean r_{sc} value in V2 was significantly larger than in V1
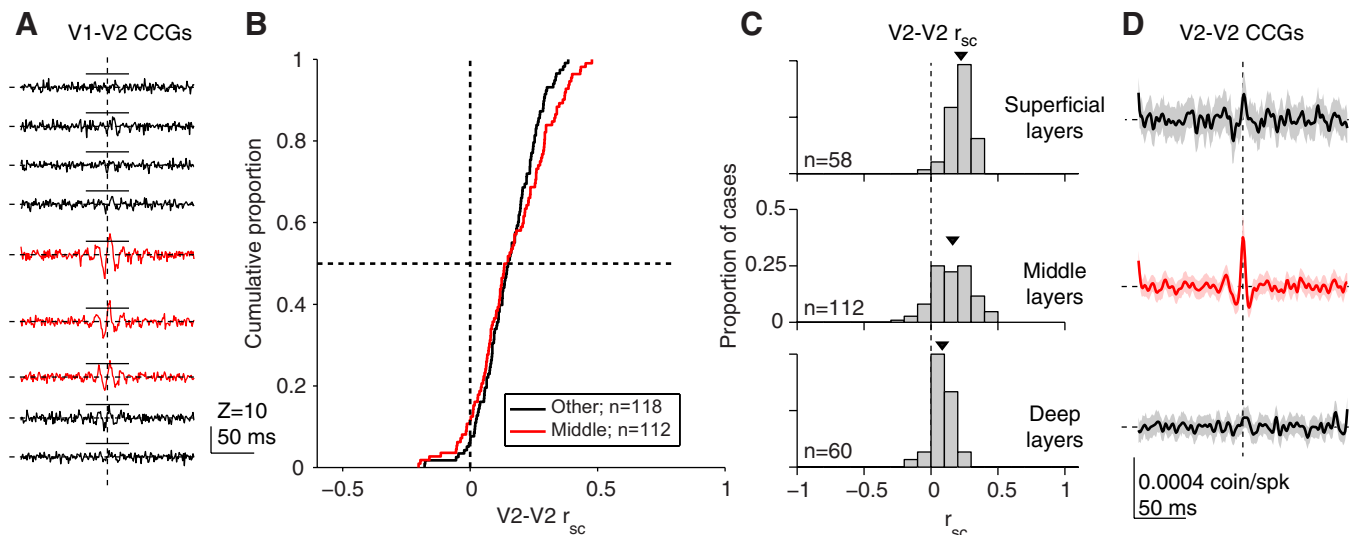
Fig. 4. Dependence of correlations in V2 on laminar location. *A*: jitter-corrected CCGs (averaged across all pairs) at 9 sites spaced by 0.25 mm, recorded in 1 V2 penetration with neurons simultaneously recorded in the superficial layers of V1. Significant sharp peaks were evident in the population-average V1-V2 CCGs at the 3rd–5th sites (indicated in red); horizontal solid lines indicate criterion level of 5 SDs. These CCGs are Z-scored, relative to the mean and SD of their values at time lags of 75–125 ms, to indicate directly which cases are deemed to be significant. The horizontal and vertical dashed lines indicate 0% synchrony and zero time lag, respectively. *B*: using the presence of sharp peaks as an indicator of the middle layers of V2, these cumulative distributions of r_{sc} show values for middle (red) and other (black) layers. *C*: histograms for r_{sc} values at superficial, middle, deep layer sites. *D*: for the same pairs shown in *C*, average jitter-corrected CCGs in the superficial, middle and deep layers. Shaded region around lines indicates ± 1 SE.

overall ($P = 2.4 \times 10^{-9}$). This was also true in the superficial and middle layer subgroups ($P = 1.0 \times 10^{-7}$ and 3.0×10^{-10}), but there was no significant difference between V1 and V2 in the deep layers ($P = 0.64$). Low frequency (0–10 Hz) LFP power recorded from the same electrodes in V2 was not significantly different between the input layers and other layers (normalized power of 0.886 ± 0.012 vs. 0.896 ± 0.010; $P = 0.66$).

We also compared the laminar dependence of spike timing correlations for V2-V2 pairs. We found broad peaks in shuffle-corrected CCGs at all three locations, consistent with the r_{sc} values shown in Fig. 4C. As in V1, synchrony was stronger in the input layers than in other layers (Fig. 4D; 8.6 ± 1.5 vs. $5.1 \pm 1.5 \times 10^{-4}$ coin./spk; $P = 0.047$ for 1-tailed t-test comparison with other layers, based on the area within $\pm$ 5 ms of zero lag). LFP gamma power was not significantly different between the input layers and other layers (0.018 ± 0.003 vs. 0.015 ± 0.002 for other layers, $P = 0.37$), although the trend was for it to be higher in the middle layers, as in V1.

Our method for determining the input layers may have misassigned recording sites to the superficial or deep layers if the number of functionally connected V1-V2 pairs was low. However, at those sites with clear evidence of direct interaction between V1 and V2, at the expected location of the input layers, we did not observe r_{sc} values different from other layers. Thus, it is not a universal principle that input layers of cortex show weak r_{sc} values.

DISCUSSION

We have shown that spike count correlations are prominent in the superficial and deep layers of V1, but near zero in the middle layers. This was reflected in the broad peak of the CCG, which was weak in the middle layers. In V2, r_{sc} in the input layers was similar to nearby layers, but synchrony was elevated, as in the middle layers of V1. Our results show that cortical layers can display distinct patterns of correlations, despite strong interlaminar circuitry linking them together. This indicates that the local network properties are a critical factor in determining the strength of correlations in neuronal populations.

We are aware of only two previously published studies that compared correlations across cortical layers. The first compared r_{sc} in the superficial and deep layers of rat auditory cortex, and found a similar strength but different spatial extent (Sakata and Harris, 2009). It did not target the middle layers, where we find the most striking differences. The second study focused on synchrony, which was weakest in the middle layers of rat somatosensory cortex (Zhang and Alloway, 2004), unlike our findings in primate V1.

In the visual system, r_{sc} is typically found to be in the range of 0.1–0.2, for well-driven neurons with similar preferences whose responses are measured over hundreds of milliseconds (Cohen and Kohn, 2011). A notable exception is a recent study which reported r_{sc} values of ~0.01 in V1 of awake, fixating macaques (Ecker et al., 2010). The authors propose this discrepancy reflects a host of artifacts in all previous studies. Our findings offer an alternative explanation - that their recordings were biased toward the input layers of V1, as in a previous study by the same group (Berens et al., 2008). More broadly, the laminar trends in correlations point to an important source of potential variation in measurements, and a critical variable

to control in future studies. We note that weak correlations have been reported in the motor cortex (Averbeck and Lee, 2006; Stark et al., 2008), further emphasizing that cortical circuits can generate different strengths of correlations.

Previous studies have established that correlations depend on response strength, the response window, the distance between recorded neurons, the quality of spike isolation and sorting, and the tuning similarity of the constituent neurons (Cohen and Kohn, 2011). The laminar differences in V1 r_{sc} values cannot be ascribed to any of these factors. In the middle layers, firing rates were higher on average than in the superficial and deep layers. We measured responses under identical stimulus conditions in each penetration, and the distance between recorded pairs was the same in all layers. We cannot rule out differences in spike isolation, although we used tetrodes and high-impedance electrodes to ensure high quality recordings (Gray et al., 1995). However, if isolation quality varied, it would be expected to be worst in the middle layers because of the high density and small size of layer 4C stellate cells. This would cause r_{sc} there to be higher than in other layers (Cohen and Kohn, 2011), opposite to our findings.

There are several, not mutually exclusive, sets of mechanisms that may contribute to the laminar dependence of correlations. First, the low r_{sc} values in V1 middle layers may arise, in part, because this network receives feed-forward input from the LGN, where responses are relatively independent (Cheong et al., 2011). This could also contribute to the drop in r_{sc} we observed at the deepest recording sites, presumably in layer 6 (Fig. 1A), which also receives substantial thalamic input. Interestingly, the koniocellular layers of the LGN, which project to the superficial layers of cortex (Chatterjee and Callaway, 2003) are more strongly correlated, particularly on slow timescales (Cheong et al., 2011). It is unlikely, however, that r_{sc} values in V1 simply reflect the properties of LGN input. If neurons pool over common inputs, as middle layer neurons do, their responses can be correlated, even if the firing of the input neurons is independent (Reid and Alonso, 1995). Furthermore, because cells in the middle layers of V1 receive common LGN input, the weak mean correlations we observe there suggest that correlation strength need not be tightly linked to common afferent input.

A second explanation for the low values of r_{sc} in the V1 middle layers is the properties of the local circuitry. Stellate cells in the middle layers have limited dendritic arbors (Lund et al., 1979; Blasdel and Lund, 1983), and do not give rise to long-range horizontal connections found in the superficial and deep layers (Lund, 1988). Feedback connections from extrastriate cortex, which target widely separated neurons, terminate in all cortical layers except the middle layers (Felleman and Van Essen, 1991; Salin and Bullier, 1995). It is thus possible that the richer, patchy recurrent circuitry outside the middle layers leads to higher r_{sc} values (Rasch et al., 2011; Litwin-Kumar and Doiron, 2012). Networks in the middle layers may conform more closely to the homogeneous random connectivity patterns that generate weak r_{sc} values in recurrent network models (Renart et al., 2010).

A third possibility is that laminar differences in correlations arise in part from differences in the intrinsic properties of neurons. For instance, neurons in layers 5 and 2/3 generate ~10 Hz rhythmic activity (Silva et al., 1991; Flint and Connors, 1996). Layer 5 neurons also generate 0.1–1 Hz oscillations (Sanchez-

Vives and McCormick, 2000; Sakata and Harris, 2009), which may propagate via patchy horizontal connections (Compte et al., 2003). While these findings cannot be linked directly to our results, they indicate laminar differences in neuronal and circuit properties that could contribute to laminar variations in correlations. A related possibility is that there is a greater diversity in the electrophysiological properties of middle-layer neurons, a factor that contributes to decorrelation in the olfactory bulb (Padmanabhan and Urban, 2010).

We have previously suggested that slow timescale correlations arise from low frequency fluctuations in responsivity (Kohn and Smith, 2005; see also Poulet and Petersen, 2008; Smith and Kohn, 2008; Kohn et al., 2009; Mitchell et al., 2009). Low-frequency LFP fluctuations are related to spike rate fluctuations in V1 (Kelly et al., 2010), and computational work suggests these fluctuations require horizontal connections (Rasch et al., 2011; Litwin-Kumar and Doiron, 2012). Consistent with this, we found a weak but significant relationship between low frequency LFP power and r_{sc}.

Whereas r_{sc} computed from full trial counts was weakest in the middle layers, synchrony was slightly higher there, suggesting distinct mechanisms generating correlations on different timescales. LFP gamma power was also high in the middle layers, and gamma power and spiking synchrony were weakly correlated in strength across layers. However, we also observed synchrony in the deep layers, where gamma was much weaker, suggesting a weak coupling between gamma and synchrony (Samonds and Bonds, 2005; Fries et al., 2008). We note that in our experiments we used gratings of an intermediate size (3–5°); gamma power is higher for larger stimuli and may display a different laminar pattern under those conditions (Gieselmann and Thiele, 2008; Jia et al., 2011; Ray and Maunsell, 2011).

The laminar trends in V1 were only partially evident in V2. Unlike V1, r_{sc} was similar in input and nearby layers. Synchrony, on the other hand, was elevated in the input layers, as in V1. The difference between V1 and V2 could reflect differences in local circuitry, neuronal properties, or the fact that feed-forward input from V1 may be more strongly correlated or show a different pattern of convergence from thalamocortical input to V1.

Given that the correlations found in cortex appear detrimental for population coding, one could ask why they exist: our results show that cortical networks can be wired to provide relatively independent responses. One possibility is that correlations arise because neurons receive diverse sources of input (e.g., from distant neurons connected via inter- or intra-areal connections). This connectivity may allow neurons to participate in diverse computations and functions, although some inputs will be irrelevant for a particular situation or computation. Because these inputs are not recruited by the stimulus or task at hand, they may provide a source of shared, fluctuating, and seemingly random drive that results in slow timescale correlations. Indeed, recent evidence suggests that training on a perceptual task leads to weaker r_{sc} values in relevant cortical neuronal populations, perhaps because these circuits become more specialized for performing this task (Gu et al., 2011).

DISCLOSURES

No conflicts of interest, financial or otherwise, are declared by the author(s).

AUTHOR CONTRIBUTIONS

Author contributions: M.A.S. and A.K. conception and design of research; M.A.S., X.J., A.Z., and A.K. analyzed data; M.A.S. and A.K. interpreted results of experiments; M.A.S., X.J., A.Z., and A.K. prepared figures; M.A.S. and A.K. drafted manuscript; M.A.S., X.J., A.Z., and A.K. edited and revised manuscript; M.A.S., X.J., A.Z., and A.K. approved final version of manuscript; X.J. and A.Z. performed experiments.

REFERENCES

Amarasingham A, Harrison MT, Hatsopoulos NG, Geman S. Conditional modeling and the jitter method of spike resampling. *J Neurophysiol* 107: 517–531, 2012.

Averbeck BB, Latham PE, Pouget A. Neural correlations, population coding and computation. *Nat Rev Neurosci* 7: 358–366, 2006.

Averbeck BB, Lee D. Effects of noise correlations on information encoding and decoding. *J Neurophysiol* 95: 3633–3644, 2006.

Bair W, Zohary E, Newsome WT. Correlated firing in macaque visual area MT: time scales and relationship to behavior. *J Neurosci* 21: 1676–1697, 2001.

Berens P, Keliris GA, Ecker AS, Logothetis NK, Tolias AS. Feature selectivity of the gamma-band of the local field potential in primate primary visual cortex. *Front Neurosci* 2: 199–207, 2008.

Blasdel GG, Lund JS. Termination of afferent axons in macaque striate cortex. *J Neurosci* 3: 1389–1413, 1983.

Bollimunta A, Chen Y, Schroeder CE, Ding M. Neuronal mechanisms of cortical alpha oscillations in awake-behaving macaques. *J Neurosci* 28: 9976–9988, 2008.

Chatterjee S, Callaway EM. Parallel colour-opponent pathways to primary visual cortex. *Nature* 426: 668–671, 2003.

Cheong SK, Tailby C, Martin PR, Levitt JB, Solomon SG. Slow intrinsic rhythm in the koniocellular visual pathway. *Proc Natl Acad Sci USA* 108: 14659–14663, 2011.

Cohen MR, Kohn A. Measuring and interpreting neuronal correlations. *Nat Neurosci* 14: 811–819, 2011.

Compte A, Sanchez-Vives MV, McCormick DA, Wang XJ. Cellular and network mechanisms of slow oscillatory activity (<1 Hz) and wave propagations in a cortical network model. *J Neurophysiol* 89: 2707–2725, 2003.

de la Rocha J, Doiron B, Shea-Brown E, Josić K, Reyes A. Correlation between neural spike trains increases with firing rate. *Nature* 448: 802–806, 2007.

De Valois RL, Albrecht DG, Thorell LG. Spatial frequency selectivity of cells in macaque visual cortex. *Vision Res* 22: 545–559, 1982.

Ecker AS, Berens P, Keliris GA, Bethge M, Logothetis NK, Tolias AS. Decorrelated neuronal firing in cortical microcircuits. *Science* 327: 584–587, 2010.

Felleman DJ, Van Essen DC. Distributed hierarchical processing in the primate cerebral cortex. *Cereb Cortex* 1: 1–47, 1991.

Fitzpatrick D, Lund JS, Blasdel GG. Intrinsic connections of macaque striate cortex: afferent and efferent connections of lamina 4C. *J Neurosci* 5: 3329–3349, 1985.

Flint AC, Connors BW. Two types of network oscillations in neocortex mediated by distinct glutamate receptor subtypes and neuronal populations. *J Neurophysiol* 75: 951–957, 1996.

Fries P, Womelsdorf T, Oostenveld R, Desimone R. The effects of visual stimulation and selective visual attention on rhythmic neuronal synchronization in macaque area V4. *J Neurosci* 28: 4823–4835, 2008.

Fries P. Neuronal gamma-band synchronization as a fundamental process in cortical computation. *Annu Rev Neurosci* 32: 209–224, 2009.

Gieselmann MA, Thiele A. Comparison of spatial integration and surround suppression characteristics in spiking activity and the local field potential in macaque V1. *Eur J Neurosci* 28: 447–459, 2008.

Gilbert CD, Wiesel TN. Clustered intrinsic connections in cat visual cortex. *J Neurosci* 3: 1116–1133, 1983.

Givre SJ, Arezzo JC, Schroeder CE. Effects of wavelength on the timing and laminar distribution of illuminance-evoked activity in macaque V1. *Vis Neurosci* 12: 229–239, 1995.

Graf ABA, Kohn A, Jazayeri M, Movshon JA. Decoding the activity of neuronal populations in macaque primary visual cortex. *Nat Neurosci* 14: 239–245, 2011.

Gray CM, Maldonado PE, Wilson M, McNaughton B. Tetrodes markedly improve the reliability and yield of multiple single-unit isolation from multi-unit recordings in cat striate cortex. *J Neurosci Methods* 63: 43–54, 1995.

Gray CM. The temporal correlation hypothesis of visual feature integration: still alive and well. *Neuron* 24: 31–47, 111–125, 1999.

Gu Y, Liu S, Fetsch CR, Yang Y, Fok S, Sunkara A, DeAngelis GC, Angelaki DE. Perceptual learning reduces interneuronal correlations in macaque visual cortex. *Neuron* 71: 750–761, 2011.

Gur M, Kagan I, Snodderly DM. Orientation and direction selectivity of neurons in V1 of alert monkeys: functional relationships and laminar distributions. *Cereb Cortex* 15: 1207–1221, 2005.

Jia X, Smith MA, Kohn A. Stimulus selectivity and spatial coherence of gamma components of the local field potential. *J Neurosci* 31: 9390–9403, 2011.

Kelly RC, Smith MA, Kass RE, Lee TS. Local field potentials indicate network state and account for neuronal response variability. *J Comput Neurosci* 29: 567–579, 2010.

Kelly RC, Smith MA, Samonds JM, Kohn A, Bonds AB, Movshon JA, Lee TS. Comparison of recordings from microelectrode arrays and single electrodes in the visual cortex. *J Neurosci* 27: 261–264, 2007.

Kohn A, Smith MA. Stimulus dependence of neuronal correlation in primary visual cortex of the macaque. *J Neurosci* 25: 3661–3673, 2005.

Kohn A, Zandvakili A, Smith MA. Correlations and brain states: from electrophysiology to functional imaging. *Curr Opin Neurobiol* 19: 434–438, 2009.

Litwin-Kumar A, Doiron B. Slow dynamics and high variability in balanced cortical networks with clustered connections. *Nat Neurosci* 15: 1498–1505, 2012.

Lund JS, Henry GH, MacQueen CL, Harvey AR. Anatomical organization of the primary visual cortex (area 17) of the cat. A comparison with area 17 of the macaque monkey. *J Comp Neurol* 184: 599–618, 1979.

Lund JS. Anatomical organization of macaque monkey striate visual cortex. *Annu Rev Neurosci* 11: 253–288, 1988.

Maier A, Adams GK, Aura C, Leopold DA. Distinct superficial and deep laminar domains of activity in the visual cortex during rest and stimulation. *Front Syst Neurosci* 4: 31, 2010.

Markram H, Toledo-Rodriguez M, Wang Y, Gupta A, Silberberg G, Wu C. Interneurons of the neocortical inhibitory system. *Nat Rev Neurosci* 5: 793–807, 2004.

Minlebaev M, Colonnese M, Tsintsadze T, Sirota A, Khazipov R. Early γ oscillations synchronize developing thalamus and cortex. *Science* 334: 226–229, 2011.

Mitchell JF, Sundberg KA, Reynolds JH. Spatial attention decorrelates intrinsic activity fluctuations in macaque area V4. *Neuron* 63: 879–888, 2009.

Nelson SB, Hempel C, Sugino K. Probing the transcriptome of neuronal cell types. *Curr Opin Neurobiol* 16: 571–576, 2006.

Padmanabhan K, Urban NN. Intrinsic biophysical diversity decorrelates neuronal firing while increasing information content. *Nat Neurosci* 13: 1276–1282, 2010.

Poulet JFA, Petersen CCH. Internal brain state regulates membrane potential synchrony in barrel cortex of behaving mice. *Nature* 454: 881–885, 2008.

Rajkai C, Lakatos P, Chen CM, Pincze Z, Karmos G, Schroeder CE. Transient cortical excitation at the onset of visual fixation. *Cereb Cortex* 18: 200–209, 2008.

Rasch MJ, Schuch K, Logothetis NK, Maass W. Statistical comparison of spike responses to natural stimuli in monkey area V1 with simulated responses of a detailed laminar network model for a patch of V1. *J Neurophysiol* 105: 757–778, 2011.

Ray S, Maunsell JHR. Different origins of gamma rhythm and high-gamma activity in macaque visual cortex. *PLoS Biol* 9: e1000610, 2011.

Reid RC, Alonso JM. Specificity of monosynaptic connections from thalamus to visual cortex. *Nature* 378: 281–284, 1995.

Renart A, de la Rocha J, Bartho P, Hollender L, Parga N, Reyes A, Harris KD. The asynchronous state in cortical circuits. *Science* 327: 587–590, 2010.

Rockland KS, Virga A. Organization of individual cortical axons projecting from area V1 (area 17) to V2 (area 18) in the macaque monkey. *Vis Neurosci* 4: 11–28, 1990.

Roopun AK, Middleton SJ, Cunningham MO, LeBeau FEN, Bibbig A, Whittington MA, Traub RD. A beta2-frequency (20–30 Hz) oscillation in nonsynaptic networks of somatosensory cortex. *Proc Natl Acad Sci USA* 103: 15646–15650, 2006.

Sakata S, Harris KD. Laminar structure of spontaneous and sensory-evoked population activity in auditory cortex. *Neuron* 64: 404–418, 2009.

Salin PA, Bullier J. Corticocortical connections in the visual system: structure and function. *Physiol Rev* 75: 107–154, 1995.

Salinas E, Sejnowski TJ. Impact of correlated synaptic input on output firing rate and variability in simple neuronal models. *J Neurosci* 20: 6193–6209, 2000.

Samonds JM, Bonds AB. Gamma oscillation maintains stimulus structure-dependent synchronization in cat visual cortex. *J Neurophysiol* 93: 223–236, 2005.

Sanchez-Vives MV, McCormick DA. Cellular and network mechanisms of rhythmic recurrent activity in neocortex. *Nat Neurosci* 3: 1027–1034, 2000.

Schroeder CE, Mehta AD, Givre SJ. A spatiotemporal profile of visual system activation revealed by current source density analysis in the awake macaque. *Cereb Cortex* 8: 575–592, 1998.

Silva LR, Amitai Y, Connors BW. Intrinsic oscillations of neocortex generated by layer 5 pyramidal neurons. *Science* 251: 432–435, 1991.

Smith MA, Kohn A. Spatial and temporal scales of neuronal correlation in primary visual cortex. *J Neurosci* 28: 12591–12603, 2008.

Smith MA, Kohn A. Laminar dependence of neuronal correlation in macaque V1. *Society for Neuroscience Abstracts*, 2009.

Stark E, Globerson A, Asher I, Abeles M. Correlations between groups of premotor neurons carry information about prehension. *J Neurosci* 28: 10618–10630, 2008.

Stoelzel CR, Bereshpolova Y, Swadlow HA. Stability of thalamocortical synaptic transmission across awake brain states. *J Neurosci* 29: 6851–6859, 2009.

Tanaka K. Cross-correlation analysis of geniculostriate neuronal relationships in cats. *J Neurophysiol* 49: 1303–1318, 1983.

Thomson AM, Lamy C. Functional maps of neocortical local circuitry. *Front Neurosci* 1: 19–42, 2007.

Van Essen DC, Newsome WT, Maunsell JH, Bixby JL. The projections from striate cortex (V1) to areas V2 and V3 in the macaque monkey: asymmetries, areal boundaries, and patchy connections. *J Comp Neurol* 244: 451–480, 1986.

Xing D, Yeh CI, Burns S, Shapley RM. Laminar analysis of visually evoked activity in the primary visual cortex. *Proc Natl Acad Sci USA* 109: 13871–13876, 2012.

Zandvakili A, Kohn A. Linear summation of feedforward corticocortical inputs. *Society for Neuroscience Abstracts*, 2010.

Zhang M, Alloway KD. Stimulus-induced intercolumnar synchronization of neuronal activity in rat barrel cortex: a laminar analysis. *J Neurophysiol* 92: 1464–1478, 2004.

Zohary E, Shadlen MN, Newsome WT. Correlated neuronal discharge rate and its implications for psychophysical performance. *Nature* 370: 140–143, 1994.